

This is an Open Access document downloaded from ORCA, Cardiff University's institutional repository: <https://orca.cardiff.ac.uk/id/eprint/136069/>

This is the author's version of a work that was submitted to / accepted for publication.

Citation for final published version:

Mashruk, Syed, Xiao, Hua and Valera-Medina, Agustin 2021. Rich-Quench-Lean model comparison for the clean use of humidified ammonia/hydrogen combustion systems. *International Journal of Hydrogen Energy* 46 (5) , pp. 4472-4484. 10.1016/j.ijhydene.2020.10.204

Publishers page: <https://doi.org/10.1016/j.ijhydene.2020.10.204>

Please note:

Changes made as a result of publishing processes such as copy-editing, formatting and page numbers may not be reflected in this version. For the definitive version of this publication, please refer to the published source. You are advised to consult the publisher's version if you wish to cite this paper.

This version is being made available in accordance with publisher policies. See <http://orca.cf.ac.uk/policies.html> for usage policies. Copyright and moral rights for publications made available in ORCA are retained by the copyright holders.



Rich-Quench-Lean model comparison for the clean use of humidified ammonia/hydrogen combustion systems

Mashruk S^a, Xiao H^b, Valera-Medina A^a

^aCardiff School of Engineering, Cardiff University, Queen's Building, Cardiff CF243AA, United Kingdom

^b School of Naval Architecture and Ocean Engineering, Guangzhou Maritime University, China

Abstract

Ammonia and hydrogen are examples of zero-carbon fuels of high interest for implementation in gas turbine technologies. However, large emissions of nitrogen oxides are still a major detrimental for the implementation of these technologies. Therefore, various techniques have been presented as potential solutions to mitigate this problem. Rich-Quench-Lean systems combined with humidified atmospheres are amongst the most promising with the reduction of emissions as a consequence of recombinations of species and lower combustion temperatures. However, limited scrutiny exists around the chemical progression of species in systems like these whilst being fuelled with ammonia blends. Furthermore, any chemical study currently faces a challenge for the selection of a chemical kinetic mechanism due to the great variety of available mechanisms for ammonia combustion, each with different characteristics for the resolution of this fuel. Thus, a Chemical Reactor Network (CRN) has been developed to numerically assess an industry scale humidified Rich-Quench Lean system, utilising five of the most used chemical kinetic models in humidified ammonia combustion whilst informing developers of the differences between those selected. The results displayed significant differences between the mechanisms as the flame progresses. Sensitivity analyses of [OH] and [NH₃] displayed similar reactions having opposing effects for these two species at various points of the burner. Quantitative Reaction Path Diagrams (QRDP) for NO showed both similarities and differences between the mechanisms in terms of paths taken and rates of production.

Keywords: Gas turbines, ammonia, hydrogen, RQL, chemical kinetic mechanisms.

1. Introduction

Ammonia as a fuel was recently included as part of the mix of fuels for the future by the International Energy Agency [1], [2]. This step comes as ammonia can be produced both from fossil fuels or most renewable sources enabling the recovery of stranded energy [3]. Ammonia has the potential for decarbonization of power production at large scale in combination with NO_x emissions relatively low and combustion products mainly consisting of nitrogen and water. However, one impediment to progress on the topic is linked to the nitrogen oxides (NO_x) and unburned species like NH₃ and hydrogen traces when used as a fuel. For example, rich ammonia combustion, known to mitigate NO_x emissions [4], [5], incurs into unacceptable unburned species. Therefore, to enable the use of ammonia at these scales,

it is crucial to employ new concepts that benefit from all the advantages of using this molecule whilst raising overall combustion efficiencies and stability.

Concurrently, the main focus of current analyses has been based on the application of ammonia for internal combustion engines [6]–[8], while large power production has just recently gained interest across the scientific community [9], [10]. Interestingly, scarce literature exists behind the use of ammonia fuelled gas turbines and their cycle efficiencies, an issue that has permeated as an obstacle for full implementation of the concept at large scale deployment. Although new concepts are under scrutiny to understand the constraints of ammonia in gas turbines for future large developments [11], [12], research is still limited with ample opportunity for improvement. Furthermore, available theoretical studies for large scale systems are also limited [13]–[15]. However, implementation of these models still rely on ideal concepts that either lack robust health and safety considerations or that fail to achieve greater efficiencies for industrial interest, thus requiring further research.

The use of ammonia fuelled gas turbines systems has been conducted experimentally with pure ammonia [16], methane-ammonia [11], [17], Coke Oven Gas (COG)-ammonia [18], and ammonia-hydrogen [4], [5], [19], showing that optimum operation for low NO_x can be achieved over rich combustion conditions with equivalence ratio values between 1.05-1.31. Emissions from these experimental campaigns, which still require further improvement, are around 10-100ppm, thus making feasible the use of ammonia as a power vector. However, emissions reduction and hydrogen utilization via easy handling chemicals such as ammonia need to be supported by the use of efficient systems. One proposal that has been continuously presented in various sources is the use of combustion techniques such as Rich-Quench-Lean (RQL) technology [20], [21]. The system, based on multi-staged combustion at different equivalence ratios, permits the reduction of emissions whilst increasing stability in the primary combustion zone [22], [23]. The high hydrogen content in the post-combustion of ammonia rich flames, observed by many [4], [15], [24], has inclined researchers and developers into the use of the technology for ammonia combustion [4], [11]. Therefore, this technique will be evaluated in this work as one of the most promising paths for ammonia combustion with low emissions.

Simultaneously, a way to augment power and efficiency is to employ humidified cycles that enable the increase of mass through the system [25]. Humidification has also been employed in systems integrated with steam reforming [26], [27] and at different compressor stages [28], thus showing great versatility. Steam injection in a cycle is considered to be an optimal way for the recovery of waste heat [29]. In addition, reduction of nitrogen oxide emissions is about 1.7 times more efficient when steam injection is applied compared to humidity increase in the inlet air [30], while in the case of the hydrogen-based mixtures the inhibiting effect of dilution by steam injection when the nitrogen oxides are formed is stronger at high flame temperatures [31]. Therefore, humidified injection technologies have

been regarded as a method for decreasing NO_x, method also employed by some groups to mitigate these emissions in ammonia-based combustion systems [4].

However, no research exists to show the chemical progression of humidified RQL technologies whilst using ammonia-based blends for combustion purposes at industrial representative scales. Being a promising solution to the emissions problem, the topic requires a study such as this to determine the feasibility of implementing a more comprehensive method of combustion for the use of ammonia by recovering as much energy as possible while minimising unwanted emissions from such a chemical.

2. Methods and Materials

2.1. Numerical Combustion Analysis

A chemical kinetic modelling tool, CHEMKIN-PRO was utilised to model chemical kinetics of the problem in hand. The PREMIX reactor [32] and the Equilibrium tool [33] were used to calculate the laminar flame speed (S_L) and adiabatic flame temperature (AFT), respectively. Solutions in this program were based on an adaptive grid of 1000 points, with mixture-averaged transport properties and trace series approximation. The calculation employed the NH₃ reaction mechanisms from Okafor et al. [34], comprised of 59 chemical species and 356 reactions. These results were used to model the RQL burner in CHEMKIN-PRO environment.

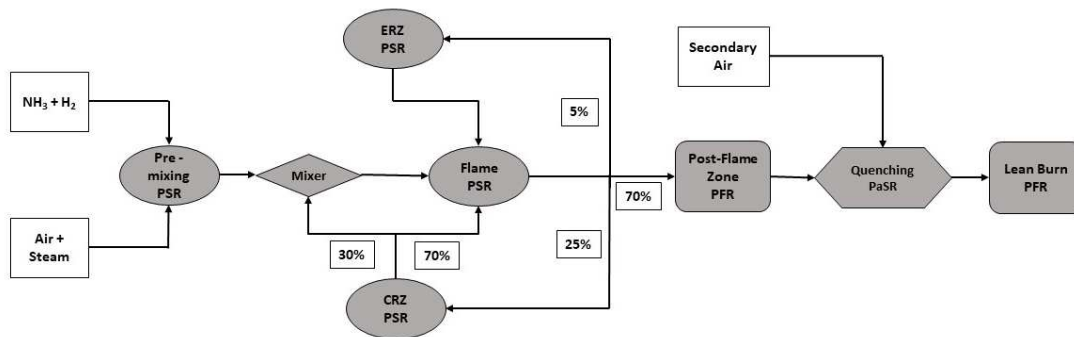


Fig 1. Chemical reaction network

A Chemical Reactor Network (CRN) was also developed, based on representative combustion geometry [35], [36] to model the RQL burner in CHEMKIN-PRO environment, Fig. 1, to numerically determine the species obtained from rich swirling flame followed by after-lean reburn. Mixing zone, flame zone, Central Recirculation Zone (CRZ) and Edge Recirculation Zone (ERZ) were modelled by individual perfectly stirred reactors (PSR) and the volume and residence time for each PSR were obtained from RANS CFD analysis [37]. The recirculation strength was determined by previous experimental campaigns that employed comparable burners [38], [39] and mass recirculation percentages for the PSR network are shown in Fig. 1. The calibration of the model for determination of heat losses

in the rich burning zone was achieved in accordance to previous experiments [5], [39], [40]. The Post-flame zone was modelled by a plug flow reactor (PFR) with one dimensional length of 30 cm. The quenching/mixing zone where the products from a rich swirling flame and secondary air, which were modelled by a partially stirred reactor (PaSR) and a PFR, respectively. Number of Monte Carlo Simulation samples (NPAR) for the PaSR was chosen to be 200 as this value provide a reasonable balance between accuracy and execution time. Reaction mechanisms from Okafor et al. [34], Glarborg et al. [41], Xiao et al. [42], Tian et al. [43] and Otomo et al. [44] were utilised to predict species formation through the system. Results from this reactor modelling were used for species sensitivity analysis. For this study, the blend that was employed was set to 70-30 (vol%) NH₃-H₂ under humidified conditions at an equivalence ratio (ER) of 1.2. The 70-30 (vol%) ratio of NH₃-H₂ have demonstrated favourable stability and reduced emissions in previous work [4] and shown to exhibit comparable behaviour to fossil fuel based flames [45]. This choice of ER was shown to produce best results for low emission values in previous numerical and experimental campaigns [4], [13]. Simulations were performed with inlet temperature of 560K and a pressure of 9.67 bar, with a secondary air flow of 3.22 kg/s with 960 K temperature to produce Turbine Inlet Temperatures ~1400 K [46]. Humidification was achieved with steam injection at a 40% fuel/steam ratio. The reference value was obtained from previous numerical studies conducted on a representative, high power (10.4MW) unit [5]. It is emphasized that there are no units of this magnitude for experimental validation yet, and these results are presented using mechanism, which have been largely validated in other works, for guidance to develop cleaner ammonia-based systems.

3. Results and Discussion

Combustion results provided theoretical details of the expected species obtained from the combustion process of this humidified ammonia-hydrogen blend in a RQL combustion system, Table 1. It is emphasized that the use of Rich combustors would deliver low NO_x emissions, but with high unburned ammonia content. Thus, the use of RQL technology offers a solution to this issue.

Results show the discrepancy between models, a known fact between modellers that is under research. However, it is clear that ammonia fraction in the rich zone is highly sensitive to $H + O_2 \leftrightarrow O + OH$ and $NH_2 + NO \leftrightarrow NNH + OH$ reactions, Fig 7. Fortunately, passed this point and into the lean reburning zone, ammonia is completely consumed in agreement with all models. Simultaneously, water concentration between cases is relatively stable, with values ranging from 32% to 14% between reaction zones. Normalised NO_x emissions (which have been normalised to 15% oxygen in accordance with British standards [47]) were obtained. Similar to unburned ammonia, nitrogen oxides do not coincide between reaction mechanisms. This is a consequence of variation in sensitivity of a few reactions, especially $NH_2 + NO \leftrightarrow N_2 + H_2O$; $NH_2 + NO \leftrightarrow NNH + OH$ and $HNO + H \leftrightarrow NO +$

H₂. Interestingly, the temperatures in the rich zone are considerably homegenous, whilst Okafor's mechanism, with the lower unburned ammonia but higher remaining hydrogen, shows the highest temperatures. At the end of the process, ~99.9% of the final products are mainly water, oxygen and nitrogen. Xiao's (based on Mathieu's mechanism[48]) and Glarborg's mechanism are fairly consistent between these species.

3.1. Sensitivity Analyses

From Table 1, Glarborg's mechanism provides the highest NO_x predictions while Otomo's mechanism gives the lowest values for the condition analysed in this study. Predictions from the other three considered mechanisms are at the same ballpark. Bearing this in mind, sensitivity analyses of the species of interest have been carried out with Glarborg, Otomo and Xiao's mechanisms.

3.1.1. [OH] Sensitivity Analysis

The OH radical is one of the most important intermediate species in hydrogen based fuels as they are found at large concentrations in the reaction zone, thus playing an important role to oxidise the fuel and reduce the ignition delay time [49]. Sensitivity analyses of [OH] have been conducted to identify key reactions involved in the production and consumption of OH radicals at four different locations in the reactor model: rich flame zone (Fig 2), end point of post-flame zone (Fig 3), beginning of lean burn zone (Fig 5) and the end point of lean burn zone (Fig 6).

The reaction $H + O_2 \leftrightarrow O + OH$ has the largest negative impact on the production of OH radicals in all three mechanisms at the rich flame zone, since all three mechanisms have the same pre-exponential factor (A) of 1.0E14 for this reaction. The reactions $NH_3 + OH \leftrightarrow NH_2 + H_2O$, $OH + H_2 \leftrightarrow H + H_2O$ and $NH_2 + NO \leftrightarrow NNH + OH$ also play an active role in the consumption of OH radicals in all three mechanisms but at different orders of magnitude. It can be clearly seen that the third body reaction $NH_3 + M \leftrightarrow NH_2 + H + M$ has the most positive impact for OH production in Xiao's mechanism but plays the least prominent role in Otomo's and does not affect [OH] at all in Glarborg's mechanism. Differences between rate constants of some key reactions can severely impact OH formation predictions. For instance, the reaction $HNO + H \leftrightarrow NO + H_2$ has a pre-exponential factor $A = 6.6E10$ in Glarborg's mechanism while in Otomo's mechanism the value is $A = 9.68E11$ and Xiao proposed a value of $A = 4.4E11$. This example demonstrates possible differences in [OH] predictions by different mechanisms, hereby variable ignition delay projections and varied production of NH_x radicals.

Table 1. Results from CHEMKIN-PRO applied to the RQL system

Mechanism	Okafor et al. [34]		Glarborg et al. [41]		Xiao et al. [42]		Tian et al. [43]		Otomo et al. [44]	
	Rich zone exhaust	Lean zone exhaust	Rich zone exhaust	Lean zone exhaust	Rich zone exhaust	Lean zone exhaust	Rich zone exhaust	Lean zone exhaust	Rich zone exhaust	Lean zone exhaust
Temperature (K)	2169	1696	2172	1493	2169	1492	2170	1492	2169	1491
NH₃ mole fraction	4.25E-06	2.68E-11	5.91E-06	-1.76E-10	5.30E-06	1.10E-09	4.65E-06	6.82E-10	2.54E-06	1.25E-11
H₂ mole fraction	0.0499	4.33E-06	0.05	3.77E-07	5.00E-02	3.44E-07	0.0499	2.79E-07	0.049851	3.71E-07
O₂ mole fraction	4.03E-06	8.91E-02	4.16E-06	1.22E-01	4.01E-06	1.22E-01	4.03E-06	1.22E-01	4.04E-06	1.22E-01
H₂O mole fraction	3.28E-01	1.99E-01	3.28E-01	1.44E-01	3.28E-01	1.44E-01	3.28E-01	1.44E-01	3.28E-01	1.44E-01
OH mole fraction	3.36E-04	2.72E-04	3.40E-04	7.26E-05	3.36E-04	7.03E-05	3.36E-04	6.09E-05	3.37E-04	7.28E-05
N₂ mole fraction	0.621342	0.711173	0.621192	0.733277	0.62130	0.73330	0.62133	0.73331	0.62139	0.73332
NO mole fraction	2.57E-04	1.37E-04	4.38E-04	1.67E-04	3.12E-04	1.20E-04	2.64E-04	1.01E-04	1.92E-04	7.30E-05
N₂O mole fraction	1.93E-08	4.61E-07	2.59E-08	4.71E-07	2.27E-08	4.97E-07	1.47E-08	6.36E-07	1.59E-08	4.77E-07
NO₂ mole fraction	4.62E-09	8.62E-07	8.00E-09	1.98E-06	5.14E-09	1.42E-06	4.74E-09	1.04E-06	3.46E-09	1.14E-06
NO (ppmv)	383	171	651	195	464	140	392	118	285	85
NO_x (ppmv)	383	172	651	198	464	142	392	120	286	87
NO – 15% O₂ (ppmv)	109	104	186	175	133	125	112	106	82	76
NO_x – 15% O₂ (ppmv)	109	105	186	178	133	127	112	108	82	78

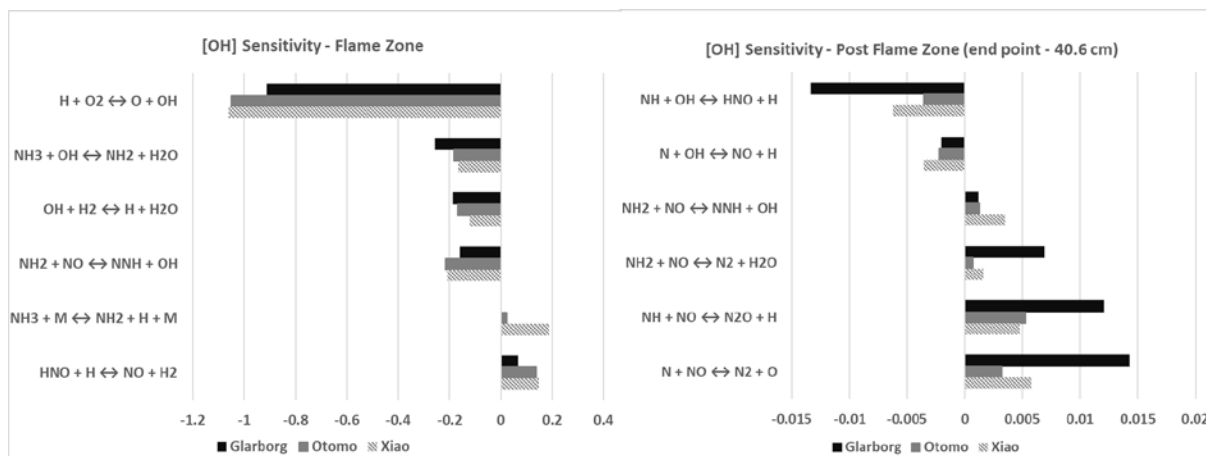


Fig 2. Computed normalized sensitivity coefficients of [OH] on net reaction rates at rich flame zone

Fig 3. Computed normalized sensitivity coefficients of [OH] on net reaction rates at the end point of post flame zone

Fig 3 compares normalized sensitivity coefficients of [OH] at the end point of the post flame zone by the three selected mechanisms. Contrary to [OH] sensitivity at the flame zone reactor, where OH radicals are not consumed as much as they are being produced, the formation of OH is highly sensitive to the presence of NO and the remaining fuel contents that lead to NH_2 formation. Moreover, the reaction $N + NO \leftrightarrow N_2 + O$ is present in all three mechanisms and has positive sensitivity coefficients, thus contributing to OH formation predictions in each of them, mostly in Glarborg's mechanism. As a consequence, Glarborg's mechanism predicts the highest OH mole fraction, as can be seen in Table 1 and Fig 4. Another reaction of interest is $NH + OH \leftrightarrow HNO + H$, which plays an important role in OH consumption and NO formation.

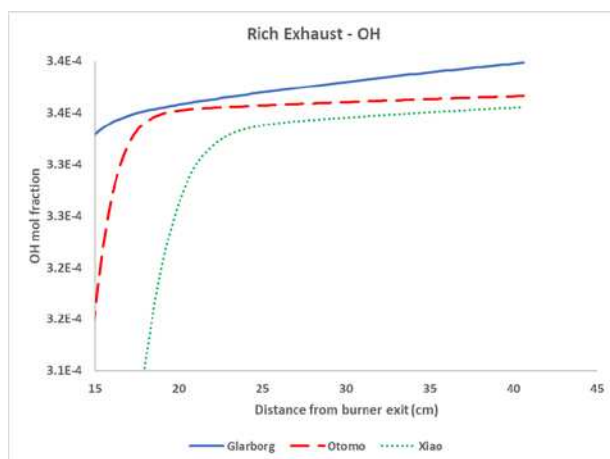


Fig 4. Comparison of OH mole fractions by different mechanisms at post-flame zone

Fig 5 and 6 compare normalized sensitivities of [OH] at the beginning and the end point of the lean burn zone, respectively, with the three mechanisms of interest. Impact of excess oxygen is clearly visible in the sensitive reactions responsible for net [OH] at the lean burn zone. The reactions $H + O_2 \leftrightarrow O + OH$ and $OH + H_2 \leftrightarrow H + H_2O$ are the most sensitive reactions at the beginning, while the $H + O_2 (+M) \leftrightarrow HO_2 (+M)$ reaction has the largest impact at the endpoint. These reactions

demonstrate the applicability of lean burning of available hydrogen from the rich zone with excess oxygen. Fig 6 also shows nearly nil OH formation at the end point by all the mechanisms as all the fuels are nearly burnt out and temperatures in this zone are considerably lower.

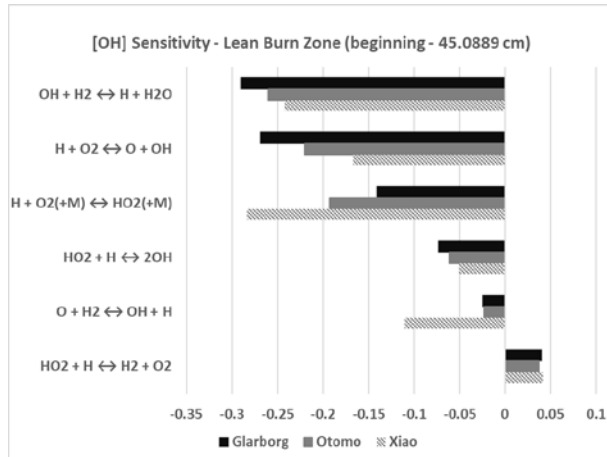


Fig 5. Computed normalized sensitivity coefficients of [OH] on net reaction rates at the beginning of lean burn zone

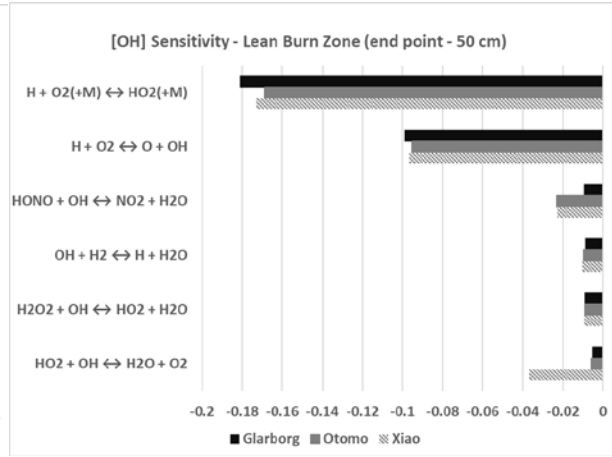


Fig 6. Computed normalized sensitivity coefficients of [OH] on net reaction rates at the end point of lean burn zone

3.1.2. [NH₃] Sensitivity Analysis

[NH₃] sensitivity analyses were also conducted to identify the sensitivity to major reactions responsible for overall [NH₃] consumption/production in this humidified RQL burner. Fig 7, 8 and 9 show the normalized sensitivity coefficients of NH₃ species at the flame zone, post flame zone and lean burn zone, respectively.

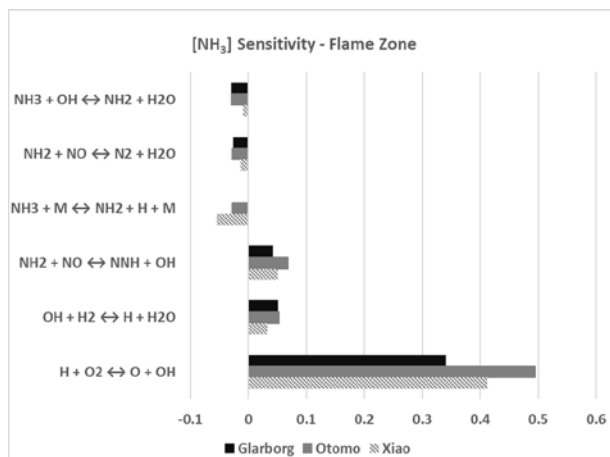


Fig 7: Computed normalized sensitivity coefficients of [NH₃] on net reaction rates at rich flame zone

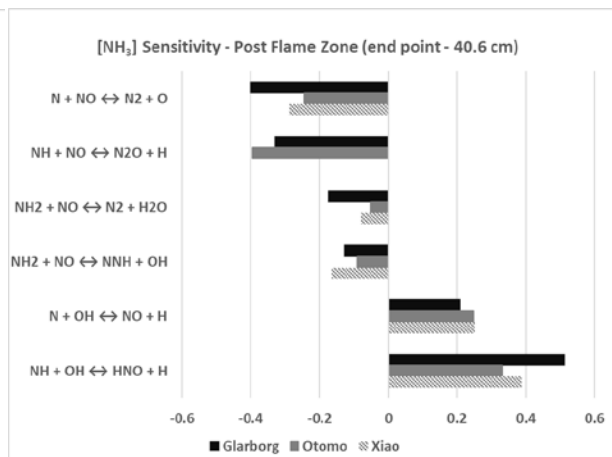


Fig 8: Computed normalized sensitivity coefficients of [NH₃] on net reaction rates at the end point of post flame zone

Comparing the sensitivity coefficients of [OH] (Fig. 2) and [NH₃] (Fig. 7) at the rich flame zone reactor, all the common reactions other than NH₃ + OH ↔ NH₂ + H₂O have opposite effects for the overall OH and NH₃ concentrations. For example, the reaction H + O₂ ↔ O + OH has the highest positive sensitivity coefficients for NH₃, opposed to the largest negative coefficients for [OH] for all the three mechanisms considered here. However, these reactions have more impact on [OH] than [NH₃], which can be concluded due to lower sensitivity coefficients for NH₃ species. NH₃ reduced to NH₂, the first main radical product of ammonia consumption, mainly by reacting with the OH and O radicals and some NH₂ radicals converts back to NH₃ by reacting with H₂. Interestingly, NO is reduced in the flame front by reacting with the NH₂ radicals through the reaction NH₂ + NO ↔ NNH + OH, reaction that boosts OH radicals. Although relatively small compared to other reactions, NH₂ + NO ↔ N₂ + H₂O is still an important contributor for ammonia consumption at the flame front. The third body reaction NH₃ + M ↔ NH₂ + H + M has the largest impact on NH₃ consumption in Xiao's mechanism but has very little or no impact in Otomo and Glarborg's mechanism.

Fig 8 compares normalized sensitivity coefficients of [NH₃] at the end point of post flame zone between the three reaction mechanisms. The reaction NH + OH ↔ HNO + H has the highest positive sensitivity coefficients in all three mechanisms but by different margins due to the differences in rate constant values. Conversely, the reaction NH + NO ↔ N₂O + H has the highest impact on NH₃ consumption in Otomo's mechanism but has lower impact in the other two mechanisms as the reaction N + NO ↔ N₂ + O has the highest impact within them. Overall, Otomo's mechanism has the lowest positive sensitivity coefficient value and Glarborg has the highest. However, Glarborg and Otomo's mechanisms have similar maximum negative sensitivity coefficient values while Xiao's mechanism has lower sensitivities. As a consequence, Otomo's mechanism predicts almost half NH₃ concentrations at the end of post flame zone compared to the other two mechanisms, as can be seen in Table 1 and Fig 10.

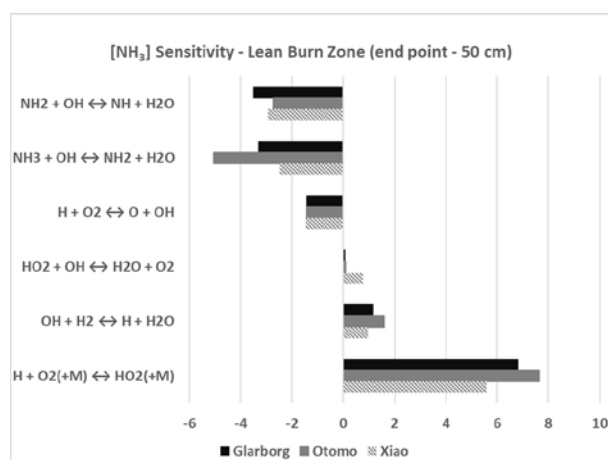


Fig 9. Computed normalized sensitivity coefficients of [NH₃] on net reaction rates at the end point of lean burn zone

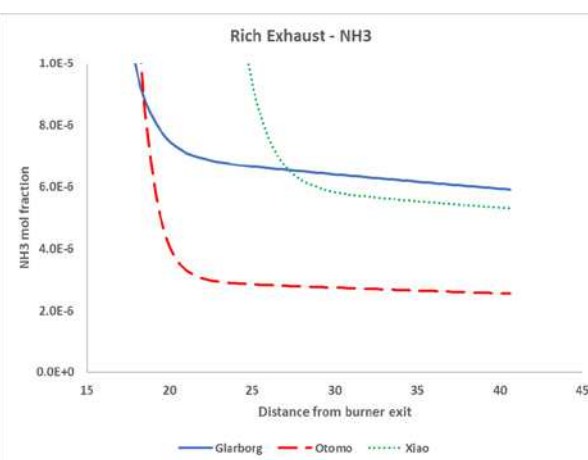


Fig 10. Comparison of NH₃ mole fractions by different mechanisms at post flame zone

Contrary to the [OH] sensitivity analysis conducted at the end point of lean burn zone (Fig. 6), the reaction $\text{H} + \text{O}_2 (+\text{M}) \leftrightarrow \text{HO}_2 (+\text{M})$ has the largest impact on NH_3 formation by all the three mechanisms (Fig. 9). NH_2 reacts with HO_2 , HONO and HNO to produce small amount of ammonia at the end point of lean burn zone. The reactions $\text{NH}_2 + \text{OH} \leftrightarrow \text{NH} + \text{H}_2\text{O}$ and $\text{NH}_3 + \text{OH} \leftrightarrow \text{NH}_2 + \text{H}_2\text{O}$ contribute largely towards any remaining NH_3 consumption at the lean burn zone in all the mechanisms but by different margins. It must be noted that the reaction $\text{NH}_2 + \text{HNO} \leftrightarrow \text{NH}_3 + \text{H}_2\text{O}$ is not included in Xiao's mechanism, hereby ammonia does not suffer considerable impacts from HNO or vice-versa in Xiao's predictions, Fig 13(c), 14(c), 19(c) and 20(c).

3.1.3. [NO] Sensitivity Analysis

NO is by far the most important by-product of NH_3 combustion due to its various adverse effects on human well-being and the climate change. Detailed [NO] sensitivity analyses have been carried out in this part of this study.

Fig 11 and 13 compare the normalized [NO] sensitivity coefficients and NO formation pathways, respectively at the flame zone by the three mechanisms. The major source of NO production at the flame zone is from HNO , according to all three mechanisms but by different rates. The reactions $\text{HNO} + \text{H} \leftrightarrow \text{NO} + \text{H}_2$ and $\text{HNO} + \text{O}_2 \leftrightarrow \text{HO}_2 + \text{NO}$ are the most prominent pathways of NO production from HNO for all three mechanisms. In addition to that, HNO also reacts with NH_2 to produce substantial NO for Glarborg and Otomo's mechanism while this reaction is not relevant in Xiao's mechanism. The third body reaction $\text{NO} + \text{H} (+\text{M}) \leftrightarrow \text{HNO} (+\text{M})$ is responsible for the reduction of NO back to HNO . Fig 15 compares the forward/reverse rate of progress from HNO to NO for all three mechanisms.

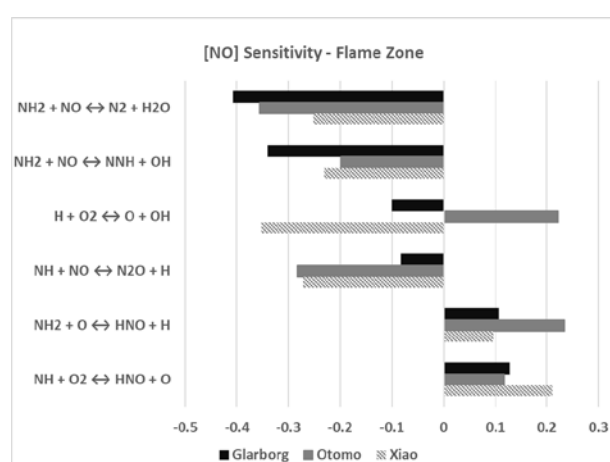


Fig 11. Computed normalized sensitivity coefficients of [NO] on net reaction rates at rich flame zone

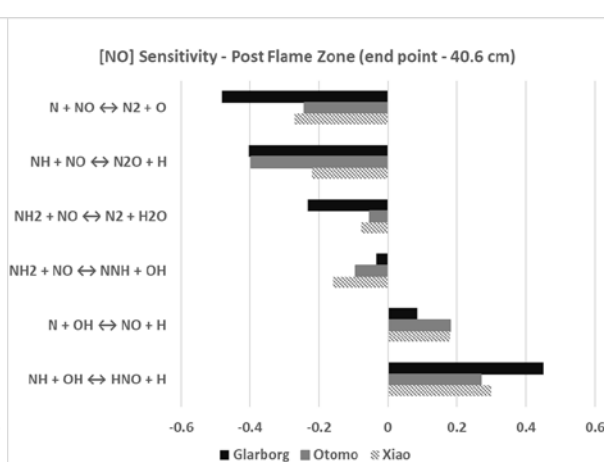


Fig 12. Computed normalized sensitivity coefficients of [NO] on net reaction rates at the end of post flame zone

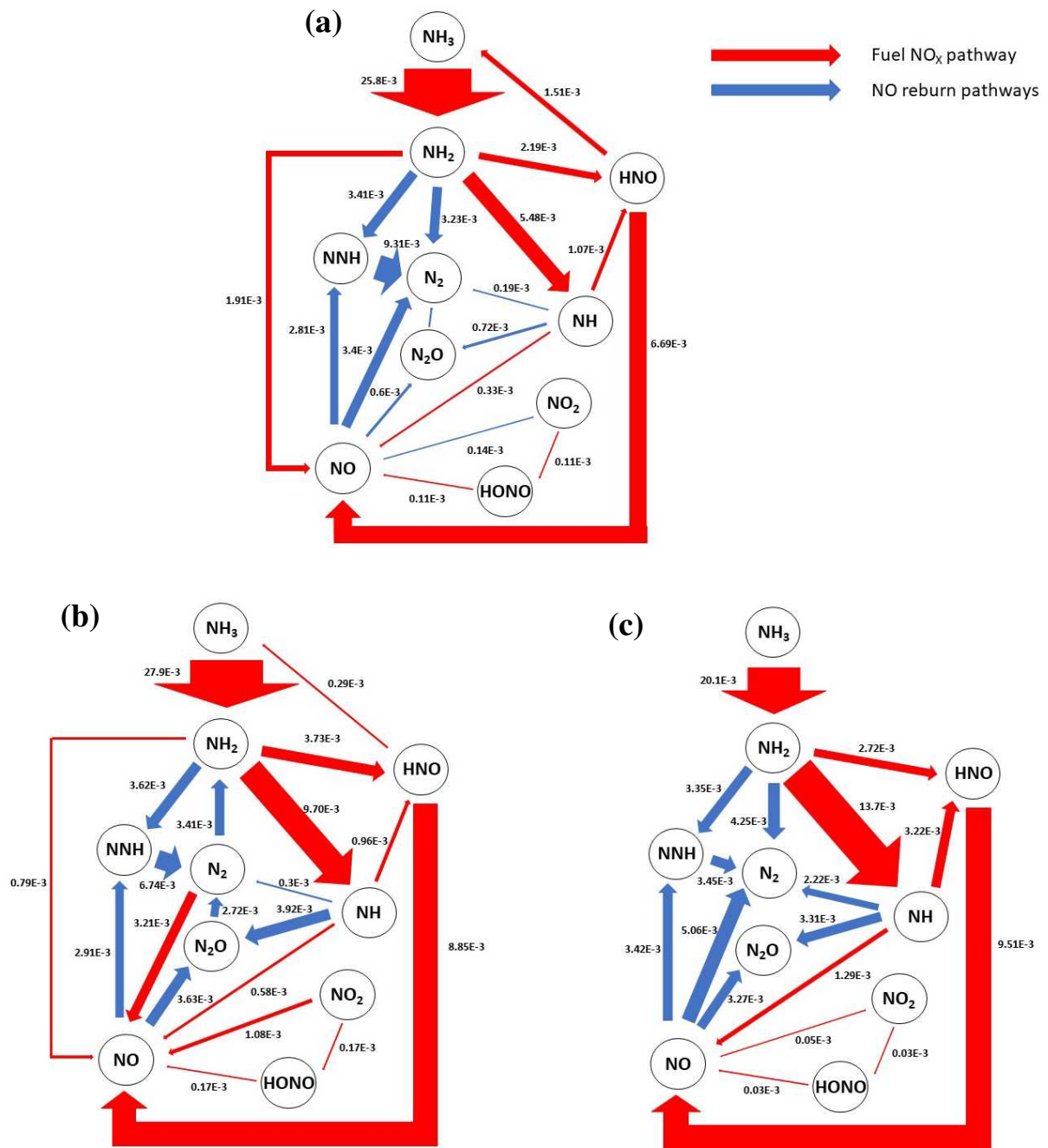


Fig 13. Quantitative reaction path diagram showing NO formation pathways at rich flame zone predicted by (a) Glarborg's mechanism, (b) Otomo's mechanism and (c) Xiao's mechanism

Interestingly, NH₂ and NH radicals react with NO to produce N₂ in Glarborg and Xiao's mechanism but N₂ reacts with O, OH and HNO to form NO in Otomo's reaction mechanism at the flame zone reactor. As a consequence, the reaction $H + O_2 \leftrightarrow O + OH$ has positive sensitivity for [NO] in Otomo's mechanism but displays negative sensitivity for the other two mechanisms. Substantial

amounts of NO are converted to NNH and N₂ through the reactions NH₂ + NO ↔ NNH + OH and NH₂ + NO ↔ N₂ + H₂O, respectively, according to all three mechanisms at flame zone. NO also reacts with NH radicals to produce N₂O and H radical, as predicted by all three mechanisms and comparatively small amounts convert back to NO by reacting with NH₂, as suggested by Glarborg and Otomo's mechanism. Glarborg and Xiao also agree on the production of NO₂ from NO in the flame zone via the reactions NO + HO₂ ↔ NO₂ + OH and NO + OH ↔ NO₂ + H.

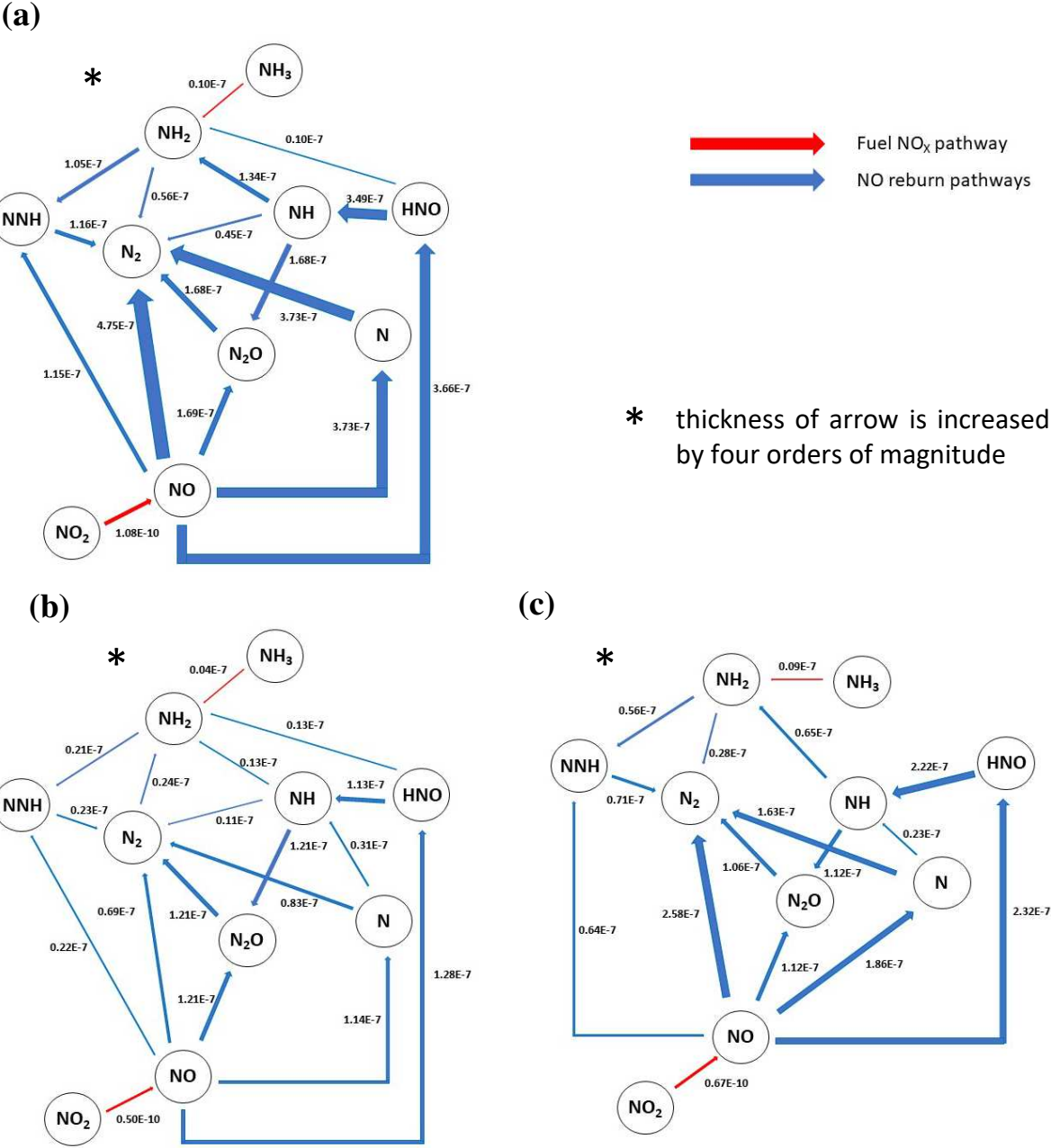


Fig 14. Quantitative reaction path diagram showing NO formation pathways at the end point of post flame zone predicted by (a) Glarborg's mechanism, (b) Otomo's mechanism and (c) Xiao's mechanism. The thickness of arrow is increased by seven orders of magnitude for NO₂ → NO.

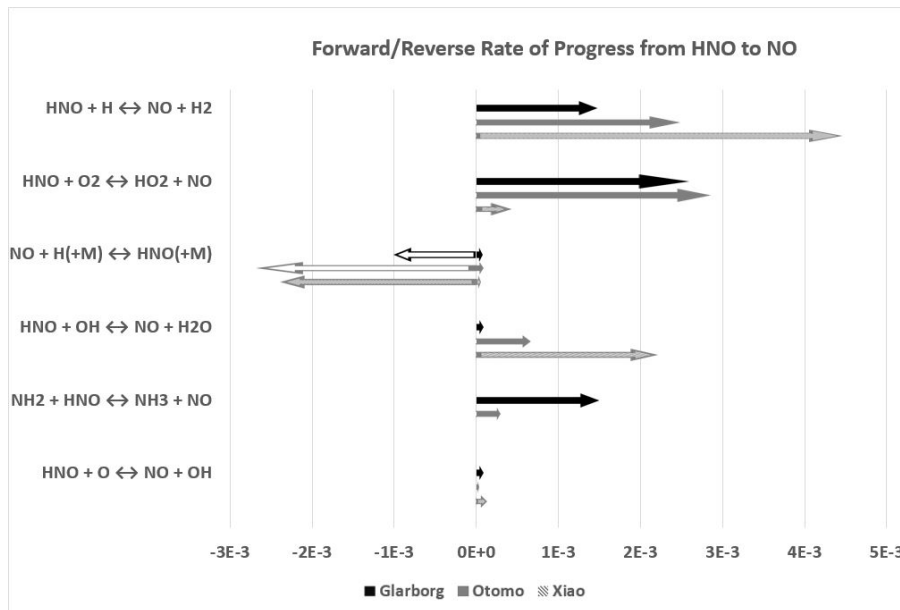


Fig 15. Forward/reverse rate of progress from HNO to NO at flame zone by Glarborg’s mechanism, Otomo’s mechanism and Xiao’s mechanism. Reverse rate of progress are shown by empty arrows with the respective color border line for Glarborg and Otomo.

Fig 12 and 14 demonstrate the differences in normalized [NO] sensitivity coefficients and NO formation pathways, respectively, at the end point of post flame zone by the three mechanisms. The main differences between the flame zone and post flame zone in terms of NO pathway is that NO is mainly being consumed at the post flame zone rather than being produced, as evidenced in Fig 16. At the end point of the post-flame zone, predictions from all three mechanisms agree with each other in terms of NO consumptions. NO reacts with NNH and converts to N₂ and HNO, while reactions with NH, NH₂ and H convert the molecule into N₂O, NNH and NH, respectively. The reaction NO₂ + H ↔ NO + OH allows small amount of NO₂ to convert back to NO.

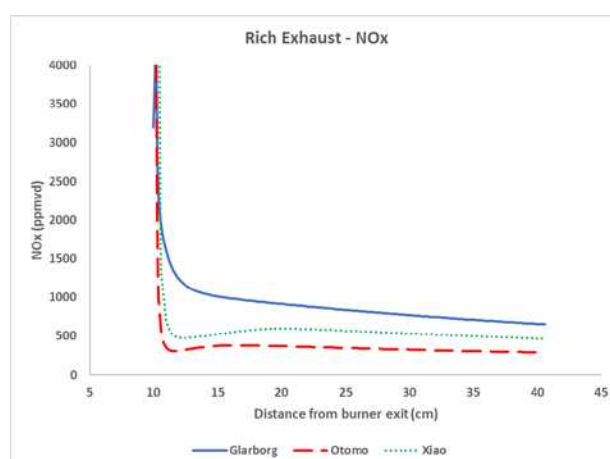


Fig 16. Comparison of NO_x production by different mechanisms at the post-flame zone.

Normalized [NO] sensitivity and NO formation pathways at the beginning of lean burn zone are compared in Figs. 17 and 19, respectively. Interestingly, NH_3 conversion to NH_2 is more significant in Xiao's and Glarborg's mechanisms, compared to Otomo's mechanism. This is due to the differences in unburned NH_3 left at the end of post flame zone, Table 1. Similar to the rich flame zone, most of the HNO converts to NO at the beginning of lean burn zone. However, the third body reaction $\text{NO} + \text{H} (+\text{M}) \leftrightarrow \text{HNO} (+\text{M})$ progresses at reverse direction, becoming a major source of NO from HNO. The reactions $\text{NO}_2 + \text{H} \leftrightarrow \text{NO} + \text{OH}$ and $\text{NO}_2 + \text{O} \leftrightarrow \text{NO} + \text{O}_2$ convert NO_2 to NO while the reactions $\text{NO} + \text{O} (+\text{M}) \leftrightarrow \text{NO}_2 (+\text{M})$ and $\text{NO} + \text{HO}_2 \leftrightarrow \text{NO}_2 + \text{OH}$ convert NO back to NO_2 . The overall balance of reaction rates of these reactions leads NO to convert into NO_2 in Glarborg's mechanism, while NO_2 converts to NO in Otomo and Xiao's mechanism, Fig 19. Substantial amount of NO converts into HONO according to all three mechanism through the reaction $\text{NO} + \text{OH} (+\text{M}) \leftrightarrow \text{HONO} (+\text{M})$. HONO reacts with OH to produce NO_2 . NO converts to N_2O through the forward reaction $\text{NH} + \text{NO} \leftrightarrow \text{N}_2\text{O} + \text{H}$ in Glarborg and Xiao's mechanism. However, this reaction operates backward along with the reaction $\text{N}_2\text{O} + \text{O} \leftrightarrow 2\text{NO}$ to convert N_2O to NO in Otomo's mechanism.

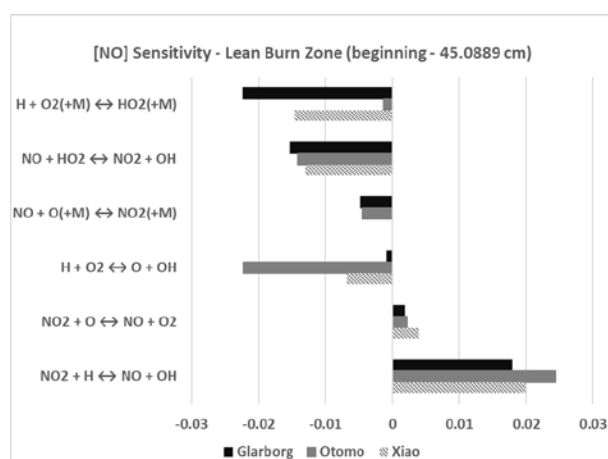


Fig 17. Computed normalized sensitivity coefficients of [NO] on net reaction rates at the beginning of lean burn zone

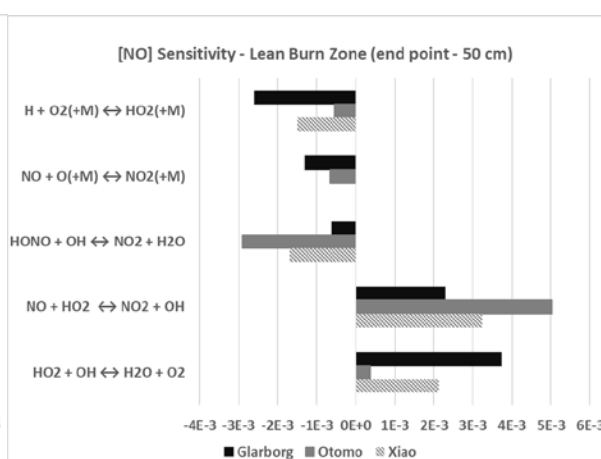


Fig 18. Computed normalized sensitivity coefficients of [NO] on net reaction rates at the end point of lean burn zone

Figures 18 and 20 compare the normalized sensitivity coefficients of [NO] and NO formation pathways, respectively, at the end point of lean burn zone by Glarborg, Otomo and Xiao's mechanism. Most of the reactions at the end point of lean burn zone are related to OH radical and excess O_2 consumption, as was shown in Fig. 6 earlier. As a consequence, the reaction $\text{HO}_2 + \text{OH} \leftrightarrow \text{H}_2\text{O} + \text{O}_2$, operating at both forward and reverse directions has a positive sensitivity coefficient. NO converts to HONO through the third body reaction $\text{NO} + \text{OH} (+\text{M}) \leftrightarrow \text{HONO} (+\text{M})$ and HONO converts to NO_2 through the reaction $\text{HONO} + \text{OH} \leftrightarrow \text{NO}_2 + \text{H}_2\text{O}$, thus have a negative sensitivity coefficient in all the mechanisms, Fig 18. In response, NO_2 reacts with OH to produce NO and HO_2 .

Finally, N_2O converts to NO and N_2 through the reactions $N_2O + O \leftrightarrow 2NO$ and $N_2O(+M) \leftrightarrow N_2 + O(+M)$, respectively.

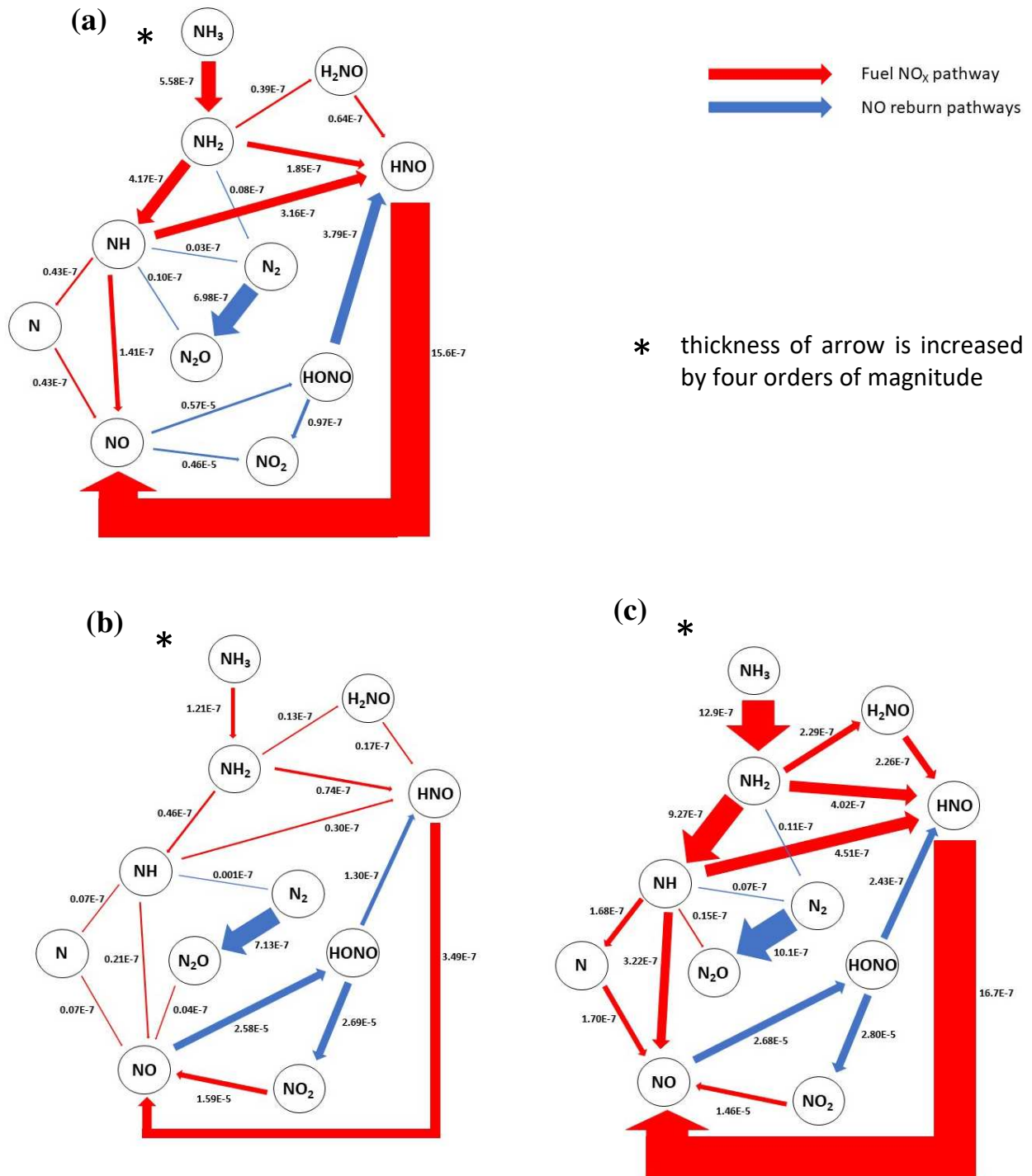


Fig 19. Quantitative reaction path diagram showing NO formation pathways at the beginning of lean burn zone predicted by (a) Glarborg's mechanism, (b) Otomo's mechanism and (c) Xiao's mechanism

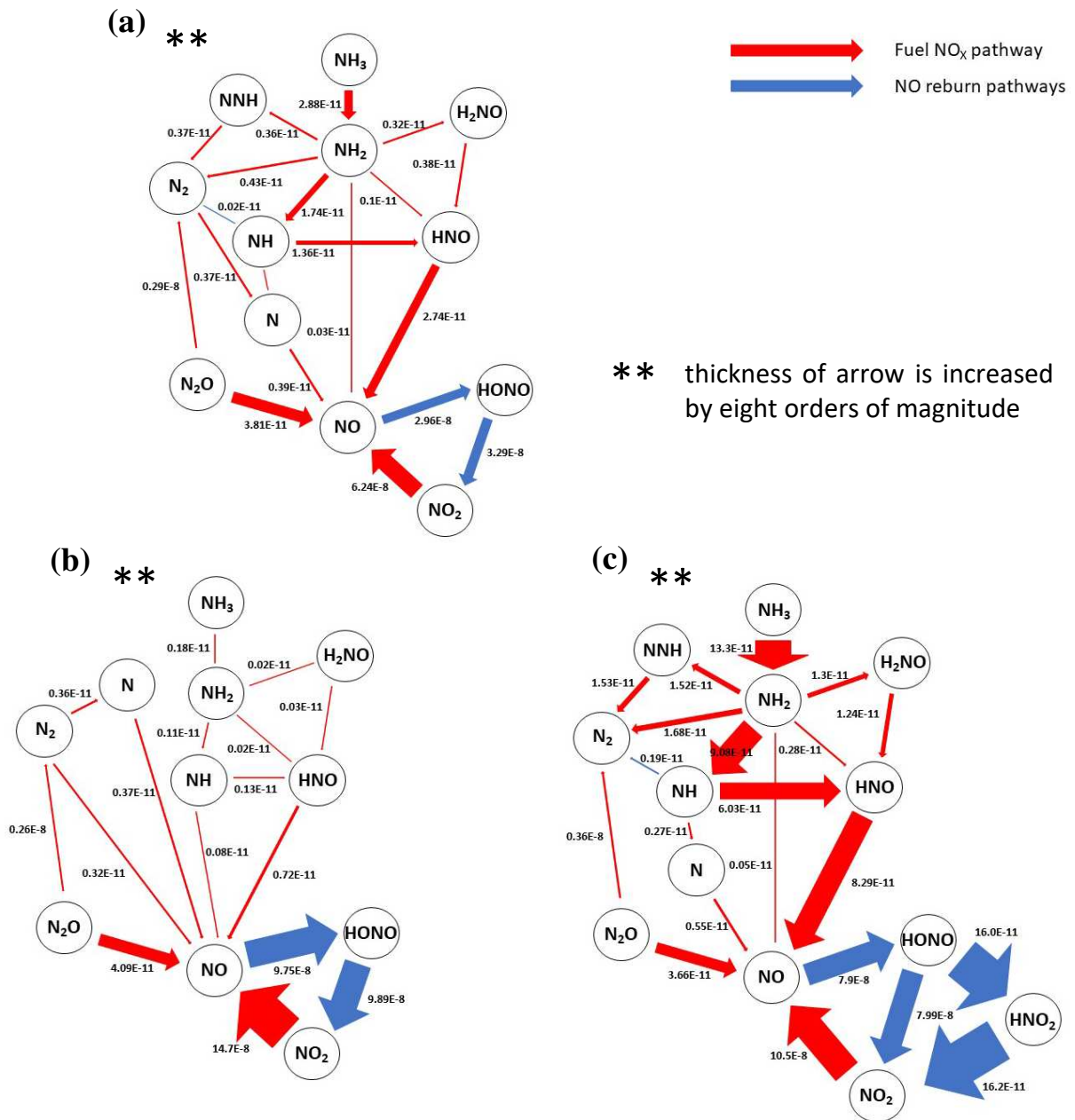


Fig 20. Quantitative reaction path diagram showing NO formation pathways at the end point of lean burn zone predicted by (a) Glarborg's mechanism, (b) Otomo's mechanism and (c) Xiao's mechanism. The thickness of arrow is increased by five orders of magnitude for $\text{NO}_2 \rightarrow \text{NO}$, $\text{NO} \rightarrow \text{HONO}$, $\text{HONO} \rightarrow \text{NO}_2$, and $\text{N}_2\text{O} \rightarrow \text{N}_2$.

As observed, the three mechanisms have different approaches to the reaction rates and paths of OH, NO and NH₃ reaction. Currently, these mechanisms are still being verified across research groups, with many claiming different progresses for the understanding of the chemical processes occurring in ammonia combustion. However, it is clear that some reactions are crucial for the mitigation of

emission and unburned ammonia. Being in accord between models, HONO, HNO and NO₂ are key molecules for the formation of NO emissions, whilst NH₂ remains an important contributor to its consumption. Whilst models agree in these terms, it is clear that the consumption of NH₃ is still a problem for further research. Meanwhile, OH appears to have good agreement between models, although its impact on the consumption of ammonia needs to be improved.

Furthermore, all these results show how the use of humidified RQL techniques for ammonia-hydrogen blends can be potentially used for low emissions combustion at ~10MW power. Different to a single Rich combustion zone, RQL technology not only offers low NO_x ~100 ppm but also provides the means to consume all remaining unburned fuels. However, further research is required to determine how radicals such as H, N and NH₂ can be employed to decrease even further the NO_x values herein found.

4. Conclusions

A numerical analysis was performed in order to inspect the efficiency and potential to implement humidified ammonia-based blends in an RQL system. Theoretical combustion results show the production of vast amounts of water with minimal traces of emissions across the post-combustion process. Pollutant emissions, i.e. NO and N₂O, in combination with unburned traces of ammonia, are only a minor fraction of the products in the flue gases entering the turbine. Although the concentration of these species tends to decrease across the combustor due to their high reactivity at high temperatures, it must be emphasized that there is still an issue that needs further development in terms of ammonia/hydrogen reactivity, with models that predict different scenarios. The importance of species such as HONO, HNO, NH₂, OH, N and H require further tuning between models to have better agreement. Moreover, radicals might offer a solution to the production of NO and further consumption of unburned ammonia, thus mitigating even more the release of unwanted emissions from these systems. However, it has been theoretically demonstrated that the use of a humidified RQL system fuelled with ammonia-hydrogen can produce flue gases consisting of 99.97% water, nitrogen and oxygen, with the consumption of most reactive species and NO_x emissions ~100 ppm at industrial large power generation, concepts that contribute to the transition towards a “zero-carbon, ultra-low climate change potential” system.

5. Acknowledgment

This work was supported at Cardiff University by EPSRC, UKRI, project no. EP/T009314/1 “Stored Ammonia For Energy (SAFE)”.

References

- [1] International Energy Agency, 'The Future of Hydrogen - Executive Report', 2019.
- [2] F. Birol, 'Hydrogen: Accelerating & Expanding Deployment', *IEA*, 2018. <https://www.nedo.go.jp/content/100885441.pdf> (accessed Sep. 10, 2019).
- [3] O. Siddiqui and I. Dincer, 'A review and comparative assessment of direct ammonia fuel cells', *Therm. Sci. Eng. Prog.*, 2018, doi: 10.1016/j.tsep.2018.02.011.
- [4] D. Pugh, P. Bowen, A. Valera-Medina, A. Giles, J. Runyon, and R. Marsh, 'Influence of steam addition and elevated ambient conditions on NO_x reduction in a staged premixed swirling NH₃/H₂ flame', *Proc. Combust. Inst.*, vol. 37, no. 4, pp. 5401–5409, 2019, doi: 10.1016/j.proci.2018.07.091.
- [5] A. Valera-Medina *et al.*, 'Premixed ammonia/hydrogen swirl combustion under rich fuel conditions for gas turbines operation', *Int. J. Hydrog. Energy*, vol. 44, no. 16, pp. 8615–8626, Mar. 2019, doi: 10.1016/j.ijhydene.2019.02.041.
- [6] C. Zamfirescu and I. Dincer, 'Using ammonia as a sustainable fuel', *J. Power Sources*, 2008, doi: 10.1016/j.jpowsour.2008.02.097.
- [7] S. Haputhanthri, J. Fleming, C. Austin, and T. Maxwell, 'Ammonia and gasoline fuel blends for spark ignited internal combustion engines', *J. Energy Resour. Technol. Trans. ASME*, vol. 137, no. 6, p. 62201, 2015.
- [8] C. Lhuillier, P. Brequigny, F. Contino, and C. Rousselle, 'Performance and Emissions of an Ammonia-Fueled SI Engine with Hydrogen Enrichment', 2019, doi: 10.4271/2019-24-0137.
- [9] A. Valera-Medina, H. Xiao, M. Owen-Jones, W. I. F. David, and P. J. Bowen, 'Ammonia for power', *Prog. Energy Combust. Sci.*, vol. 69, pp. 63–102, 2018, doi: 10.1016/j.pecs.2018.07.001.
- [10] H. Kobayashi, A. Hayakawa, K. D. K. A. Somarathne, and E. C. Okafor, 'Science and technology of ammonia combustion', *Proc. Combust. Inst.*, Nov. 2018, doi: 10.1016/j.proci.2018.09.029.
- [11] E. C. Okafor *et al.*, 'Control of NO_x and other emissions in micro gas turbine combustors fuelled with mixtures of methane and ammonia', *Combust. Flame*, vol. 211, pp. 406–416, Jan. 2020, doi: 10.1016/j.combustflame.2019.10.012.
- [12] A. Valera-Medina, 'Stored Ammonia for Power (SAFE)', 2020. www.safeammonia.com (accessed Apr. 16, 2020).
- [13] M. Guteša Božo, M. O. Viguera-Zuniga, M. Buffi, T. Seljak, and A. Valera-Medina, 'Fuel rich ammonia-hydrogen injection for humidified gas turbines', *Appl. Energy*, vol. 251, p. 113334, Oct. 2019, doi: 10.1016/j.apenergy.2019.113334.
- [14] M. Guteša-Bozo and A. Valera-Medina, 'Novel Humidified Ammonia/Hydrogen Gas Turbine Cycles', 2019.
- [15] M. Keller, M. Koshi, J. Otomo, H. Iwasaki, T. Mitsumori, and K. Yamada, 'Thermodynamic evaluation of an ammonia-fueled combined-cycle gas turbine process operated under fuel-rich conditions', *Energy*, 2020.
- [16] N. Iki *et al.*, 'Nox reduction in a swirl combustor firing ammonia for a micro gas turbine', 2018, doi: 10.1115/GT201875993.

- [17] A. Valera-Medina *et al.*, ‘Ammonia–methane combustion in tangential swirl burners for gas turbine power generation’, *Appl. Energy*, vol. 185, 2017, doi: 10.1016/j.apenergy.2016.02.073.
- [18] S. G. Hewlett, A. Valera-Medina, D. G. Pugh, and P. J. Bowen, ‘Gas Turbine Co-Firing of Steelworks Ammonia with Coke Oven Gas: A Fundamental and Cycle Analysis’, in *Proceedings of the ASME Turbo Expo*, 2019, pp. GT2019-91404.
- [19] A. Valera-Medina, D. G. Pugh, P. Marsh, G. Bulat, and P. Bowen, ‘Preliminary study on lean premixed combustion of ammonia-hydrogen for swirling gas turbine combustors’, *Int. J. Hydrog. Energy*, 2017, doi: 10.1016/j.ijhydene.2017.08.028.
- [20] A. H. Lefebvre and D. R. Ballal, *Gas Turbine Combustion*, 3rd Editio. CRC Press, 2010.
- [21] R. C. Rocha, M. Costa, and X.-S. Bai, ‘Combustion and Emission Characteristics of Ammonia under Conditions Relevant to Modern Gas Turbines’, *Combust. Sci. Technol.*, pp. 1–20, 2020.
- [22] J. Li, J. Chen, L. Yuan, G. Hu, and J. Feng, ‘Flow Characteristics of a Rich-Quench-Lean Combustor-Combined Low-Emission and High-Temperature Rise Combustion’, *Int. J. Aerosp. Eng.*, 2019, doi: 10.1155/2019/4014120.
- [23] B. Ge, Y. Ji, S. Zang, Y. Yuan, and J. Xin, ‘Investigation of the combustion performance in a three-nozzle RQL combustor’, 2016, doi: 10.1115/GT2016-57308.
- [24] K. D. K. A. Somarathne, S. Hatakeyama, A. Hayakawa, and H. Kobayashi, ‘Numerical study of a low emission gas turbine like combustor for turbulent ammonia/air premixed swirl flames with a secondary air injection at high pressure’, *Int. J. Hydrog. Energy*, vol. 42, no. 44, pp. 27388–27399, Nov. 2017, doi: 10.1016/j.ijhydene.2017.09.089.
- [25] P. Chiesa, G. Lozza, and L. Mazzocchi, ‘Using hydrogen as gas turbine fuel’, *J. Eng. Gas Turbines Power*, 2005, doi: 10.1115/1.1787513.
- [26] Z. Huang, C. Yang, H. Yang, and X. Ma, ‘Off-design heating/power flexibility for steam injected gas turbine based CCHP considering variable geometry operation’, *Energy*, 2018, doi: 10.1016/j.energy.2018.09.126.
- [27] C. Zhang, X. Wang, C. Yang, and Z. Yang, ‘Control Strategies of Steam-injected Gas Turbine in CCHP System’, 2017, doi: 10.1016/j.egypro.2017.03.461.
- [28] W. De Paepe, M. Renzi, M. M. Carrero, C. Caligiuri, and F. Contino, ‘Micro gas turbine cycle humidification for increased flexibility: Numerical and experimental validation of different steam injection models’, *J. Eng. Gas Turbines Power*, 2019, doi: 10.1115/1.4040859.
- [29] W. De Paepe, P. Sayad, S. Bram, J. Klingmann, and F. Contino, ‘Experimental Investigation of the Effect of Steam Dilution on the Combustion of Methane for Humidified Micro Gas Turbine Applications’, *Combust. Sci. Technol.*, 2016, doi: 10.1080/00102202.2016.1174116.
- [30] S. Shahpouri and E. Houshfar, ‘Nitrogen oxides reduction and performance enhancement of combustor with direct water injection and humidification of inlet air’, *Clean Technol. Environ. Policy*, 2019, doi: 10.1007/s10098-019-01666-4.
- [31] S. Göke and C. O. Paschereit, ‘Influence of steam dilution on NO_x formation in premixed natural gas and hydrogen flames’, 2012, doi: 10.2514/6.2012-1272.

- [32] R. J. Kee, J. F. Grcar, M. D. Smooke, J. A. Miller, and E. Meeks, 'PREMIX: a Fortran program for modeling steady laminar one-dimensional premixed flames', *Sandia Natl. Lab. Rep.*, no. SAND85-8249, 1985.
- [33] S. Gordon and B. J. McBride, 'Computer program for calculation of complex chemical equilibrium compositions rocket performance incident and reflected shocks, and Chapman-Jouguet detonations', *Comput. Program Calc. Complex Chem. Equilib. Compos. Rocket Perform. Incid. Reflected Shocks ChapmanJouguet Detonations*, 1971.
- [34] E. C. Okafor *et al.*, 'Experimental and numerical study of the laminar burning velocity of CH₄-NH₃-air premixed flames', *Combust. Flame*, vol. 187, pp. 185-198, Jan. 2018, doi: 10.1016/j.combustflame.2017.09.002.
- [35] D. Pugh *et al.*, 'An Investigation of Ammonia Primary Flame Combustor Concepts for Emissions Reduction with OH*, NH₂* and NH* Chemiluminescence at Elevated Conditions', *Combust. Symp. Consid.*, 2020.
- [36] Pugh, D. Valera-Medina, A. Bowen, P. Giles, A. Gokepte, B. Runyon, J. Morris, S. Hewlett, S. Marsh, R., 'Emissions Performance of Staged Premixed and Diffusion Combustor Concepts for an NH₃/Air Flame With and Without Reactant Humidification', presented at the Turbomachinery Technical Conference and Exposition, Jun. 2020.
- [37] M. Viguera-Zuniga, M. Tejada-del-Cueto, J. Vasquez-Santacruz, A. Herrera-May, and A. Valera-Medina, 'Numerical Predictions of a Swirl Combustor Using Complex Chemistry Fueled with Ammonia/Hydrogen Blends', *Energies*, vol. 13, no. 2, p. 288, 2020, doi: doi.org/10.3390/en13020288.
- [38] A. Valera-Medina, N. Syred, and P. Bowen, 'Central recirculation zone visualization in confined swirl combustors for terrestrial energy', *J. Propuls. Power*, vol. 29, no. 1, 2013, doi: 10.2514/1.B34600.
- [39] S. Mashruk, 'NO Formation Analysis using Chemical Reactor Modelling and LIF Measurements on Industrial Swirl Flames', PhD Thesis, Cardiff University, 2020.
- [40] A. Valera-Medina, A. Giles, D. Pugh, S. Morris, M. Pohl, and A. Ortwein, 'Investigation of Combustion of Emulated Biogas in a Gas Turbine Test Rig', *J. Therm. Sci.*, 2018, doi: 10.1007/s11630-018-1024-1.
- [41] P. Glarborg, J. A. Miller, B. Ruscic, and S. J. Klippenstein, 'Modeling nitrogen chemistry in combustion', *Prog. Energy Combust. Sci.*, vol. 67, pp. 31-68, Jul. 2018, doi: 10.1016/j.peccs.2018.01.002.
- [42] H. Xiao and A. Valera-Medina, 'Chemical Kinetic Mechanism Study on Premixed Combustion of Ammonia/Hydrogen Fuels for Gas Turbine Use', *J. Eng. Gas Turbines Power*, vol. 139, no. 8, p. 081504, 2017, doi: 10.1115/1.4035911.
- [43] Z. Tian, Y. Li, L. Zhang, P. Glarborg, and F. Qi, 'An experimental and kinetic modeling study of premixed NH₃/CH₄/O₂/Ar flames at low pressure', *Combust. Flame*, vol. 156, no. 7, pp. 1413-1426, 2009.
- [44] J. Otomo, M. Koshi, T. Mitsumori, H. Iwasaki, and K. Yamada, 'Chemical kinetic modeling of ammonia oxidation with improved reaction mechanism for ammonia/air and ammonia/hydrogen/air combustion', *Int. J. Hydrog. Energy*, vol. 43, no. 5, pp. 3004-3014, 2018.
- [45] F. J. Verkamp, M. C. Hardin, and J. R. Williams, 'Ammonia combustion properties and performance in gas-turbine burners', in *Symposium (International) on Combustion*, 1967, vol. 11, no. 1, pp. 985-992.

- [46] A. M. Y. Razak, Ed., 'Chapter 2: Thermodynamics of gas turbine cycles', in *Industrial Gas Turbines*, Woodhead Publishing, 2007, pp. 50–59.
- [47] British Standard, 'BS ISO 11042-1:1996. Gas Turbines-Exhaust Gas Emission', 1996.
- [48] O. Mathieu and E. L. Petersen, 'Experimental and modeling study on the high-temperature oxidation of Ammonia and related NO_x chemistry', *Combust. Flame*, vol. 162, no. 3, pp. 554–570, Mar. 2015, doi: 10.1016/j.combustflame.2014.08.022.
- [49] J. Warnatz, U. Maas, and R. W. Dibble, *Combustion: Physical and Chemical Fundamentals, Modeling and Simulation, Experiments, Pollutant Formation*, 4th ed. Berlin Heidelberg: Springer-Verlag, 2006.